

Robust Inner Knuckle Print Recognition System Using DenseNet201 and InceptionV3 Models

Haitham Salman Chyad

Tarek Abbas

Follow this and additional works at: <https://ijcsm.researchcommons.org/ijcsm>



Part of the [Computer Engineering Commons](#)



ORIGINAL STUDY

Robust Inner Knuckle Print Recognition System Using DenseNet201 and InceptionV3 Models

Haitham Salman Chyad^{1b}*, Tarek Abbas^{1b}

Innov'COM, National School of Electronics and Telecommunications of Sfax, University of Sfax, Tunisia

ABSTRACT

Texture features and stability have generated significant interest in biometric recognition. The inner knuckle print is distinctive and difficult to fake, making it extensively used in individual identification, criminal investigation, and various other domains. In recent years, the rapid progress of deep learning technology has created new prospects for internal knuckle recognition. This paper proposes a robust inner-knuckle-print recognition system (RIKP-RS) depending on two deep learning (DL) models. This paper focuses on the key components of the inner surface of the hand namely the little finger, ring finger, middle finger, index finger, and thumb finger that are used for human identification. Using the new segmentation method, rely on the Hands Landmark Module (MediaPipe Module) to detect components that have important biometric features. By Considering the inner knuckle print (IKP) as a texture, this study adopts two effective models: The DenseNet201 model and the InceptionV3 model to extract distinctive features from every modality. Uses all the key points of inner knuckle prints (IKP) of ten fingers for concatenated fusion recognition of all the features extracted by these models. Ultimately, these features are classified by different similarity metrics that are employed to compute the matching procedure for each model individually. A dataset of 11,076K hands with left and right palms was used to evaluate the proposed system. The system achieved the best performance on this dataset with a rank-1 score of 98.45% on the denseNet201 model, a rank-1 score of 99.81% on the inceptionV3 model for all left IKP, a rank-1 score of 96.68% on the denseNet201 model, and rank-1 score of 98.32% on the inceptionV3 model for all right IKP. These results cover the inceptionV3 model for all concatenated fusion recognition. In terms of performance, the RIKP-RS outperforms the most advanced inner knuckles pattern (IKP) recognition systems.

Keywords: Inner knuckle print (IKP) recognition, Feature extraction (FE), Fusion features, Deep learning, Densnet201 model, InceptionV3 model, MediaPipe module

1. Introduction

In recent years, there has been considerable scholarly interest in novel biometric identification technologies that leverage the distinctive features of the human hand. Apart from conventional palm print, palmar vein, and finger vein recognition, knuckle print recognition has emerged as one of the most prominent technologies [1–4]. Initially, knuckle prints have rich texture and line features that can achieve excellent recognition accuracy [5]. The second, knuckle prints are easy to capture and can only be acquired with standard low-resolution cameras.

The widespread use and low cost of cameras nowadays make it convenient to promote and use knuckle print recognition [6, 7]. To create a high-precision recognition system, the knuckle print can also be paired with the palm print, hand shape, and finger vein. Lastly, unique features of knuckle prints, like line distance and orientation, may improve their applicability for large-scale retrieval tasks, especially when significant data gathering is possible [8–10].

Knuckle prints are the textured areas or curving muscle lines found on a person's first, second, and third finger joints. It is distinct from other biological characteristics like fingerprints and palm prints

Received 1 December 2024; revised 28 February 2025; accepted 9 March 2025.
Available online 12 April 2025

* Corresponding author.

E-mail addresses: dr.haitham@uomustansiriyah.edu.iq (H. S. Chyad), tarek.abbes@enetcom.usf.tn (T. Abbas).

<https://doi.org/10.52866/2788-7421.1245>

2788-7421/© 2025 The Author(s). This is an open-access article under the CC BY license (<https://creativecommons.org/licenses/by/4.0/>).

and has its own set of rules. These areas include the hand's knuckles' delicate structure and texture features, which are useful for identifying and recognizing specific individuals. Knuckle prints are a valuable and independent biometric recognition technique since they differ from fingerprints and palm prints in certain aspects, such as shape. Its lines are somewhat thicker and the tiny grooves between them are marginally wider than those of fingerprints. The knuckle print's texture structure is often simple, consisting primarily of curved, wavy, and horizontal or oblique straight lines. In contrast to the palm print, its line is typically shorter, has fewer lines than the palm print's primary line, and is also comparatively single-directional [11].

Human knuckle prints are found on all ten fingers and can be classified into two categories: palm knuckle prints and hand-back knuckle prints. While the knuckles on the palm are referred to as the inner knuckles, the knuckles on the back of the hand are also known as the dorsal knuckles. There are additional sources of information for biometric identification because the two categories of knuckle prints have different positions and features. By examining and contrasting the dorsal and inner knuckles of the hand, more thorough and precise individual recognition can be accomplished. Even if identical twins have the same fingerprint, their textures are thought to be distinct and unchanging throughout time [11–13].

Three different flexor muscle lines, which roughly correspond to three knuckles, are typically found in a finger. The main knuckle prints are those that are located in the middle and provide a lot of information. The first little knuckle line is the region nearest the nail tip of the flexor muscle line. The second little knuckle is the region that is nearest to the palm's flexor muscle line. The position and features of these several knuckle sites vary, offering more precise information for identifying individual fingers. Finger feature recognition can be made more thorough and precise by examining and contrasting the main - knuckle print (MKP), the first little -knuckle print (FL-KP), and the second little -knuckle print (SL-KP).

Deep learning (DL) is a branch of artificial intelligence that utilizes neural networks (NN) with many layers to automatically learn and extract patterns from large datasets. It offers many benefits, comprising enhanced accuracy, the ability to handle complex and large-scale data, and reduced reliance on manual feature extraction (FE). DL enables systems to adapt and improve over time, making it ideal for tasks such as image recognition (IR), natural language processing (NLP), and predictive analytics [14]. DL in inner knuckle print (IKP) recognition is an emerging field in biometric technology that leverages advanced neural

networks (NN) to analyze the unique patterns found within the inner knuckle area. Unlike conventional techniques that often rely on fingerprints or palm prints, inner knuckle print (IKP) recognition offers an additional layer of security by utilizing these subtle, intricate patterns. By training deep learning (DL) models on high-resolution images of inner knuckle print (IKP), researchers aim to enhance the accuracy and reliability of identification systems, making this technology a promising addition to the field of biometric recognition [10].

According to the current research, no studies have been conducted using all ten fingers on both hands and combining them to identify the inner knuckle print. Our work proposes a robust inner-knuckle-print recognition system, named RIKP-RS based on the DenseNet201 model and Inception V3 model to extract texture features for all inner-knuckle-prints (IKP) in both hands. To obtain these texture features, the first step is to select a dataset that contains the entire hand. In order to detect the inner knuckle print (IKP), this step is given to blur the hand image, convert it to HSV color space, perform morphological operations (Dilation and Erosion), median filtering, and the Mediapipe Module. The second step is two deep learning (DL) models using fine-tuned hyperparameters to extract texture features. The final step is to compare each model separately using a set of similarity metrics. The inner-knuckle print recognition system is the main focus of this paper. The following are the most significant contributions of this study:

1. Proposing a novel segmentation method to obtain the inner knuckle print (IKP) Using the Mediapipe Module which is fast and universal. Mediapipe's hand-tracking module's sophisticated landmark detection and skeletal modelling allow for segmenting inner knuckles. Region segmentation, median filters, blurring, HSV color space conversion, and morphological operations (Dilation and Erosion) can extract inner knuckle patterns from finger phalanges.
2. Prove an effective segmentation method by evaluating actual and predicate samples for the inner knuckle print to impact the robustness of an image recognition system. This method improved boundary clarity, reduced noise, and adapted to illumination and hand position differences.
3. Investigate many fundamental convolution neural network (CNN) models to achieve optimal performance in texture feature extraction. Afterwards, fine-tune using the highest performing models, DenseNet201 and InceptionV3. Fine-tuning improves texture features that enhance robustness against illumination and hand

variations. Utilizing pre-trained weights speeds up training and prevents overfitting for effective biometric recognition.

4. Propose concatenated fusion inner knuckle print features for all fingers (little, ring, middle, index, and thumb) for both hands, as well as extract them separately to differentiate among them and determine the strength of concatenated fusion features which was not investigated yet in the literature. The Concatenated inner knuckle print features improve recognition accuracy by combining patterns from many fingers. Integrated feature vectors from multiple knuckle regions provide more discriminative information, enhancing robustness against hand orientation, illumination, and texture noise. The fused representation improves biometric recognition by diversifying features and lowering false matches.
5. Propose similarity metrics (Hamming distance (HamD) similarity, Jaccard distance (JaD) similarity, Braun-Blanquet (BB) similarity, and Bray-Curtis (BC) similarity) to obtain a robustness performance recognition system by comparing texture features for each model individually. As far as we know, this is the first study to compare features using this metric in a biometric context. Distance similarity in inner knuckle pattern recognition improves feature stability, matching accuracy, and distortion reduction.

The subsequent sections of this paper are structured as follows: [Section 2](#) reviews the previous works. [Section 3](#) presents the materials and methods. [Section 4](#) highlights the evaluation results for each model. [Section 5](#) provides the comparison and discussion. [Section 6](#) discusses the conclusion.

2. Previous works

IKP recognition only became popular a few years ago in the field of biometric technologies. Face print, palm print, outer FKP, and IKP recognition have all been the focus of many studies. With these, a variety of feature extraction and description techniques have been applied, with varying degrees of accuracy and performance. A novel inner-knuckle-print recognition system (IKP) was proposed by Liu et al. [15]. To extract features, an improved local binary pattern (LBP) technique was utilized. This technique diverges from traditional 3×3 neighborhood encoding by instead capturing features within four specific neighborhoods aligned horizontally on the right and left. Once the encoded image is generated, it undergoes decomposition into multilayer binary images, with cross-correlation employed for precise feature matching.

The results showed that the system, when applied to 2,000 images of 100 different persons, achieved good accuracy and robustness. Another system for examining the identification of an individual based on inner knuckle print (IKP) was put up by Bahmed and Mammam [16]. To extract features, an enhanced method called “Average Line Local Binary Pattern” (ALLBP) for the IKP region. Utilizing Hamming Distance (HamD) to confirm image matching has proven to be an effective system. Experimental results on the standard contact-free dataset have shown the highest accuracy in the system. Another system for inner knuckle print (IKP) recognition was developed by Rajini and Prabha [17], which highlights on local line binary pattern (LLBP) to extract features after suppressing noise through the use of image filtering. For efficient classification use two methods “artificial neural network” (ANN) and “support vector machine” (SVM) for IKP recognition. An accuracy of 89% and 97% classification was obtained by SVM and ANN classifier with 100 images taken from 100 various individuals. Viswanathan et al. [18] created an Inner-Knuckle-Print (IKP) recognition system that depends on a two-finger image contactless, which employs the LBP approach to extract features from IKP. For matching using the Back-Propagation (BP) algorithm which achieved the best accuracy with 100 images. A technique integrating global features that represent “principal component analysis” (PCA) and local features that represent “Local binary pattern” (LBP) was developed by Li W [19] to extract the texture features. The developed technique can increase both the recognition rate and the recognition speed by combining the high accuracy of local refined matching with the quick speed of global coarse matching that is achieved with 1500 images. An identification system reliant on inner-knuckle-print (IKP) was developed by Tao et al. [20], where a new extraction method proposed by modified maximum curvature point (MMCP) is used to obtain a central IKP area line pattern that is robust to changes in illumination. To match features, use the normalized Hamming Distance (HamD). Experiments were conducted on a dataset comprising 1987 IKP images from 209 various fingers, with 8–10 images from each finger showing good performance. Sadik et al. [21] designed an identification system reliant on Center inner knuckle prints (CIKP). To extract features and matching employ the two techniques: Neighboring Direction Indicator (NDI) and Chi-Square. The experiments conducted on the Sfax-Miracle dataset achieved the highest outcomes for both Equal Error Rate (EER) and Best Identification Rate (BIR). To identify the person, Nezhadian and Rashidi [22] adopted two techniques “Gabor Wavelet Filtering” (GWF) and

“Wavelet Energy” (WE) to extract features. These features are classified by several classification techniques such as “K-Nearest Neighbor” (KNN), “Fuzzy K-Nearest Neighbor” (FKNN), “Parzen Window” (PW), and “Support Vector Machine” (SVM). The experiment was done at Hong Kong Polytechnic University using non-contact 3D/2D hand images and included 177 persons. The 2D Gabor Filter (GF) along with proper scale orientations, was used by Kazemtarghi et al. [23] to extract features for the inner side of the knuckle print (ISKP). SVM classifier applies to these features. The high accuracy rate was achieved using 177 individuals. Jaswal et al. [24] examined novel features based on an inner knuckle print (IKP) recognition system, whereby texture features depend on local direction patterns and knuckle distance depends on geometrical features. Utilizing a K-NN classifier to classify features for each class. The system achieved the highest performance in terms of CRR (96%), and EER (3.45%) applied to 720 images, collected over a period of three months. A novel identification system that relied on the geometric features of the IKP was introduced by Zhu et al. [25] First, the system extracts the “region of interest” (ROI) from the IKP and then uses the K-means clustering algorithm to determine ROI centroid. Lastly, feature matching using “Euclidean Distance” (ED) based on “K-nearest neighbor” (KNN) algorithm. The system achieved high results (98.39%) using a small dataset collected. The system has difficulty identifying IKP features, as it is not done accurately which impacts the system performance. Another system for analyzing an individual’s identity based on the Finger Inner Surfaces (FISs) was presented by Al-Nima et al. [26], Initially, an innovative strategy that employs a variety of image processing techniques is used to segment the FIS. Second, a feature extraction technique reliant on the “Coefficient of Variance” (CV) and “Wavelet Discrete Transform” (DWT) is used. Lastly, an intelligent software application is used to verify the FIS’s effectiveness, and “Neural Network” (NN) performance is used in this study. CASIA multi-spectral palm images have been used to evaluate the FIS patterns for the left and right hands. This study yielded the following results: the “False Acceptance Rate” (FAR) was 0.3333%, and the “False Rejection Rate” (FRR) was 0.8889%. Authentication of individuals based on extracted finger texture (FT) Proposed by Al-Nima et al. [27], It involves extracting the lower details of the image, subtracting this information from the original image, extracting the upper features from the same image, and combining these features to the resultant image (the subtracted image). As an intelligent classifier for recognition, a Probabilistic Neural Network (PNN) is used once the resultant feature image has been seg-

mented. The experiment was conducted on the Hong Kong Polytechnic University database version 1.0, where the suggested approach performs better. Furthermore, the Equal Error Rate (EER) of 4.07% produced the most efficient IFE outcomes. Xue et al. [28] presented an identification system based on a hand inner knuckle pattern (HIKPS). To extract features using a “Convolution Neural Network” (CNN). The system achieved a recognition rate of (95.2%) using a fully connected layer and the softmax, as the system does not have the diversity of the training and testing samples determined for CNN which may affect the usage model for various hand types. Afif [29] proposed a novel system for individual gender recognition based on hand images. CNN was used to extract features to feed SVM for feature classification. The system achieved a classification rate of (0.942 and 0.973) for palm and dorsal hand images with 11K hand datasets. The system suffers from some complexity in training the model due to the use of CNN with SVM classifiers, which is a challenge in real-time applications. Most current deep learning (DL) research utilizing segmentation techniques demands extensive data labeling for network training, a process that proves difficult with large datasets. Notably, the literature of inner knuckle prints in hand images remains underexplored within biometric systems. One possible explanation for this oversight is the dynamic nature of IKP. While numerous recognition methods for inner knuckle prints exist in the literature, none are flawless; each presents distinct limitations, often stemming from challenges inherent in computer vision (CV) and machine learning (ML). Consequently, there remains significant potential for advancement, particularly in the application of DL to IKP recognition.

3. Materials and methods

This work proposes a robust inner-knuckle-print recognition system depending on two deep learning (DL) models. The system utilizes pre-training models: The DenseNet201 and Inception V3 architectures for inner-knuckle-print (IKP) recognition. These models were pre-trained on the 11,076K hands dataset; fine-tuning is required to utilize them with the datasets used in this work.

3.1. Dataset

The “11-k Hands” dataset is used in this work to evaluate a convolutional neural networks (CNN) performance. 11076 hand images from 190 individuals are included in the 11k Hands collection, which contains both palmar and dorsal perspectives. The images

show hands in a range of positions, including closed, half-closed, and widely open. With the hands about at the same distance from the camera, each image in this dataset was captured utilizing a USB document camera with a 1600×1200 -pixel resolution [30].

Moreover, since the subject of this work is inner knuckle print (IKP), the 2624 left and 2845 right palmar images have been chosen. For the training and validation of the fine-tuned model, 55,055 and 49,856 segmented images from the left and right palmar in the 11k Hands dataset, respectively, were utilized. For training and validation, the dataset was split into 70% and 30%, respectively.

3.2. Deep learning models

Deep learning is the subject of recent study and is mostly utilized in biometrics and computer vision [31, 32]. Its robustness and higher recognition scores are the reasons for its success. Two distinct baseline models are thoroughly evaluated in this work. A couple of these models include DenseNet201 and InceptionV3. These models were selected because of their successful application in computer vision. To make each model suitable for the number of classes utilized in the tests, fine-tuning is included. A brief discussion of each of these different models will be provided in each subsequent subsection.

3.2.1. DenseNet201 model

One of the more sophisticated designs in the Dense Convolutional Networks (DenseNet) family is DenseNet201. The training of neural networks is made more efficient and effective by its extensive connection and 201 layers. Utilizing the aggregate knowledge of all previous levels, DenseNet201 allows each layer to accept input from all preceding layers. In comparison to conventional architectures, this dense connection dramatically improves gradient flow, mitigates the vanishing gradient issue, makes feature reuse more efficient, and uses fewer parameters [33–35]. The enhanced gradient propagation guarantees that gradient deterioration will not impact the training of increasingly deeper networks. Furthermore, DenseNet201 reduces overfitting by introducing a regularization effect as a result of the recurrent use of features [33, 36].

3.2.2. InceptionV3 model

InceptionV3 is an advanced architecture that uses creative module design to expand the breadth and depth of neural networks while preserving computing efficiency. The Inception module, which performs convolutions of several kernel sizes (1×1 , 3×3 , and 5×5) in parallel, is the central component of

InceptionV3. The network is very good at processing complicated images because of its multi-scale convolution method, which enables it to capture features at various spatial resolutions. By breaking down more complex convolutional operations into smaller ones, the Inception modules are made to minimize the computational load while still attaining good performance with a minimal number of parameters. InceptionV3 is an effective tool for image classification problems because it strikes a compromise between computational efficiency and the capacity to gather fine-grained spatial information [37].

3.3. Proposed system

In our system, named RIKP-RS, This study employs two efficient models: The DenseNet201 model and the InceptionV3 model. Enhanced through the fine-tuning of feature extraction (FE). The system passes the primary phases: Preprocessing, Feature Extraction (FE), Fusion Features for IKP, and Matching. Multiple steps are employed in each phase to identify every test sample and determine whether they are all from the identical individual. Fig. 1 depicts the framework of the proposed system.

3.3.1. Pre-processing phase

This phase uses the hand image to identify the inner knuckle patterns (IKP) for five fingers. The method used in this work to identify the location of a hand area, such as inner knuckle patterns (IKP), is hand posture estimate utilizing the hand's module (MediaPipe Module). This model's major points are used to identify the hand's primary components. Resizing the original manual image to 224×224 produced the best localization key points result. A variety of processing steps are used to implement the IKP detection method, including:

1. Applying a blurring step to the hand image: By adding a filter to an image, more noise can be eliminated and the image becomes blurrier. In image processing, image blurring is an essential element [38, 39].
2. Convert to HSV color space step: This step's goal is to determine the hand image's skin region by first converting the RGB to HSV color space and then using specific skin area determination techniques [40–42].
3. Apply morphological operations step: These are a group of procedures that process images using shapes. An output image is created when a structural element has been added to an input image. Dilation and Erosion are two of the most basic morphological processes [43–45].

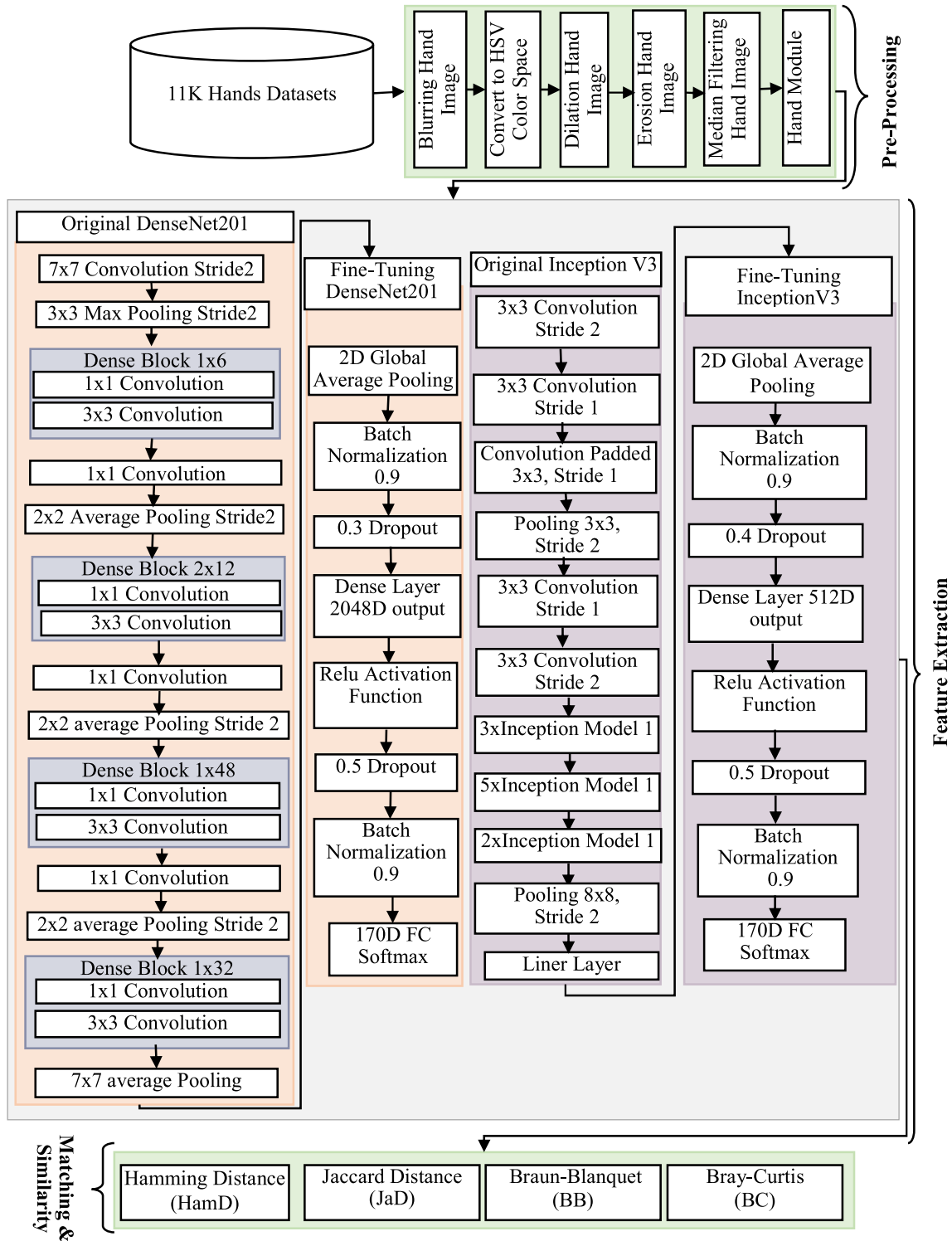


Fig. 1. Proposed framework for RIKP-RS.

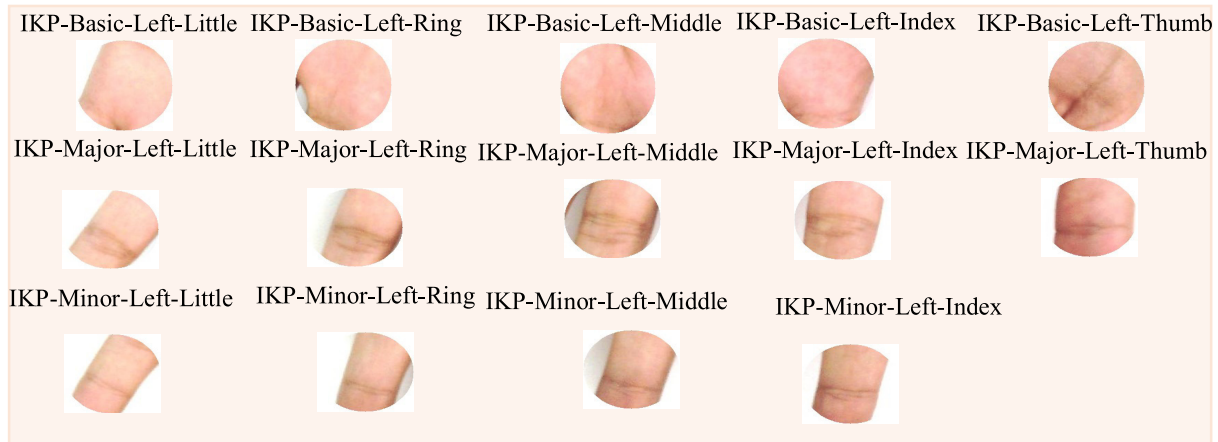


Fig. 2. Show a sample of sub-images of the key points of the hand.

Table 1. DenseNet201 model and inception V3 model hyper parameters value.

Hyper Parameters	DenseNet201 Model	Inception V3 Model
	Value	
Input Size	224 × 224	224 × 224
Batch Size	16	16
Seed	1337	42
Optimizer	Adam	Adam
Learning-rate	1e-2	1e-3
Epochs	100	100
Loss Function	Binary-Cross Entropy	Binary-Cross Entropy
Dense	2048	512
Total parameters	26,988,797 (Use 11K Dataset)	22,948,829 (Use 11K Dataset)
Trainable Parameters	8,654,781 (Use 11K Dataset)	13,958,717 (Use 11K Dataset)
Non-Trainable Parameters	18,334,016 (Use 11K Dataset)	8,990,112 (Use 11K Dataset)

4. Utilize the median filtering step: This is a great step to reduce this type of noise. The entire image is scanned by the filtering approach using a tiny matrix, like the 3×3 . It then recalculates the value of the center pixel using the median of all the values inside the matrix [46–48].
5. The MediaPipe Module step is used: This technique is quite accurate in tracking hands and fingers. Nine 2D hand landmarks are inferred from a single frame using machine learning (ML) [49, 50].

By the perform of four processing processes, the hand's key points will be cropped into sub-images, as illustrated in Fig. 2 Each hand has 14 different parts for both hands, including:

1. (5) for the IKP-Basic
2. (5) for the IKP-Major (as known as IKP-Center)
3. (4) for the IKP-Minor

3.3.2. Feature extraction (FE) phase

In order to achieve high-performing results, feature extraction (FE) is a prerequisite for every pattern

recognition system. To differentiate between different patterns, it is essential to obtain characteristics of unevenness and distinctiveness [51, 52]. Therefore, the feature vector (FV) of all IKP was extracted in this study using the suggested fine-tuning of the Dense Net201 model (refer to Fine-Tuning in Fig. 1) and the fine-tuning of the InceptionV3 model (refer to Fine-Tuning in Fig. 1). Table 1 displays the hyper-parameter and parameter combinations selected for the DenseNet201 and Inception V3 models. First, the pre-trained model's Inception V3 and DenseNet201 were loaded. After that, a convolution was carried out using a 224×224 input image, freezing the ImageNet weights for transfer learning (TL) and feature extraction (FE). The first 700 levels of the original DenseNet201 model were frozen. Some of the 48 layers in Inception V3 should be frozen for this present work. The Global Average Pooling (GAP), Flatten, and Fully Connected (Dense) layers are then used and fine-tuned. For RIKP-RS recognition, this study utilized an output layer with a softmax activation function. To avoid overfitting, this work improved the training process by including a dropout layer and a batch normalization layer.

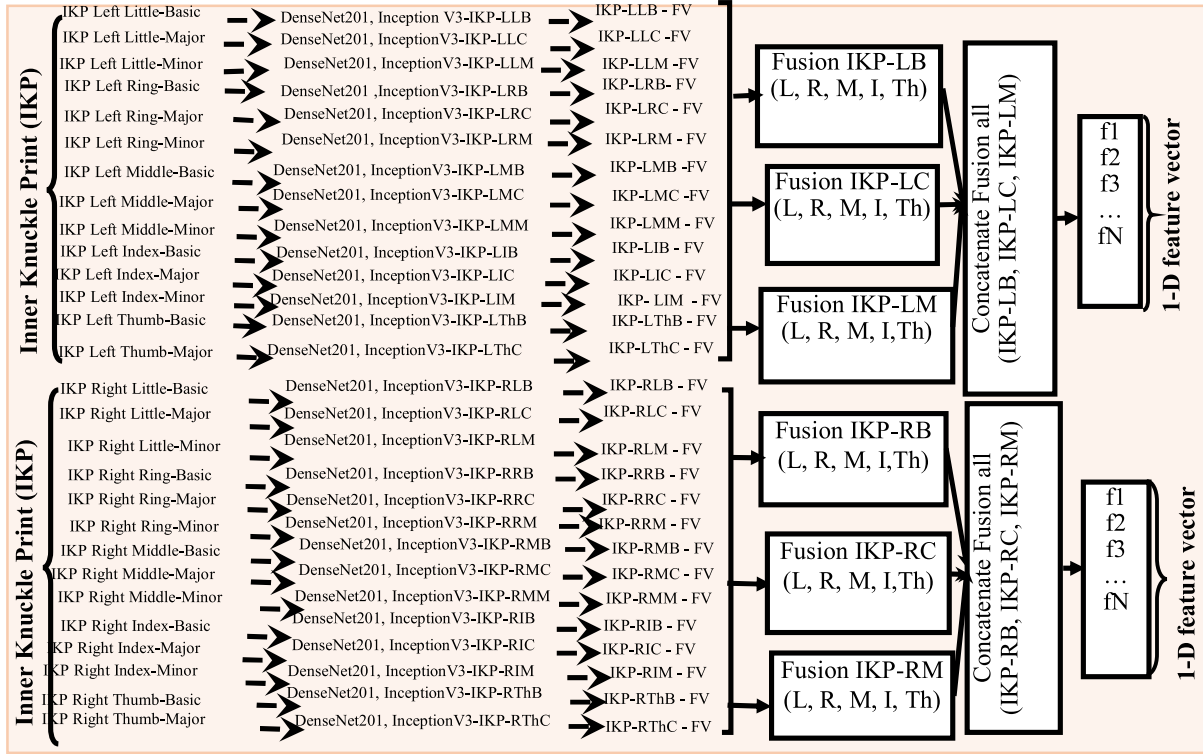


Fig. 3. Shows the proposed feature-level fusion for the IKP's location.

3.3.3. Fusion features for IKP phase

Combining feature vectors (FV) for all the inner knuckle prints of the five-finger regions. In order to improve the RIKP-RS, a feature-level fusion method for feature extraction (FE) is suggested that uses the InceptionV3 and DenseNet201 models for distinct IKP features. In the fusion phase generates three feature fusions and extracts separately for IKP-Basic, IKP-Center, and IKP-Minor for per fingers as well as concatenated fusion inner knuckle print features for all fingers (little, ring, middle, index, and thumb) for both hands in 11-k Hands dataset.

- Feature Vector Fusion for IKP-Left-Basic: (IKP-Left Little-Basic) + (IKP-Left Ring-Basic) + (IKP-Left Middle-Basic) + (+ IKP-Left Index-Basic) + (IKP-Left Thumb-Basic)
- Feature Vector Fusion for IKP-Left-Major: (IKP-Left Little-Center) + (IKP-Left Ring-Center) + (IKP-Left Middle-Center) + (IKP-Left Index-Center) + (IKP-Left Thumb-Center)
- Feature Vector Fusion for IKP-Left-Minor: (IKP-Left Little-Minor) + (IKP-Left Ring-Minor) + (IKP-Left Middle-Minor) + (IKP-Left Index-Minor)
- Concatenated Fusion all: (IKP-Left-Basic) + (IKP-Left-Major) + (IKP-Left-Minor)

The same concatenated feature vector fusion of (Basic, Major, and Minor) is performed on the right hand. Regarding the IKP regions, the results of the suggested feature-level fusion for the location in the context of hand-based biometric recognition are presented in Fig. 3.

3.3.4. Matching and similarity phase

In order to try to address pattern recognition difficulties, similarity, and distance (dissimilarity) metrics are crucial [53]. To determine the distance or resemblance between two items at their respective positions, a variety of mathematical procedures are employed [54]. The basic model feature extractor previously presented is employed in the four-phase along with a number of metrics. The optimal recognition outcomes are then utilized for the ensuing fine-tuning stage to further improve performance. According to the similarity metric, which is the inverse of the distance metric between two vectors, the degree of similarity raises as the distance between them decreases and vice versa. In this work, these hand parts are initially mapped onto feature spaces using feature extractors. The second step involved matching individuals based on hand components by utilizing similarity criteria. The Bray-Curtis (BC), Braun-Blanquet (BB), Jaccard (JaD), and Hamming (HamD) metrics are used to evaluate the suggested

Algorithm 1. the Proposed RIKP-RS

Input: Data Set 11-K Hands

Output: Individual Recognition

BEGIN

Step1: Read the original Hand image

Step2: FOR each row (I) from 1 to image height: 224 pixels

Step3: FOR each column (J) from 1 to image width: 224 pixels

Step4: **Preprocessing Phases**

Step4-1: While Hand image (I) is available do

Step4-2: Segmenting the Inner Knuckle Prints

Step4-3: Convert to HSV color space

Step4-4: Apply morphological operations (dilation and erosion)

Step4-5: Apply median filtering

Step4-6: Use hands Landmark Model (Mediapipe Module)

Step4-7: **END FOR (J)**

Step4-8: **END FOR (I)**

Step4-9: return Final Result

Step5: Create a database with sub-images of every component.

Step6: **Feature Extraction Phases**

Step6-1: for $p \leftarrow 1$ to 14 do

Step6-2: Separate the database into testing, validation, and training classes.

Step6-3: Set the network configuration (DLNN apply Fine-tuning DenseNet201, Fine-tuning InceptionV3)

Step6-4: Create augmentation images

Step6-5: Use specific epochs to train.

Step6-6: Determine the network weight (W) has the highest validation accuracy and F1 Score

Step6-7: Using W, extract the features from the pairings (a) and (b).

Step7: **Matching and Similarity Phases**

Step7-1: Compute the distances using the respective equations:

Step7-2: if

Hamming Distance (HamD) compute the number of differing bits between features using [Eq. \(1\)](#)

Step7-3: then

Jaccard Distance (JaD) measures the similarity between two sets and is computed using [Eq. \(2\)](#)

Step7-4: **END**

Step7-5: if

Braun-Blanquet (BB) measures the similarity between two sets using equation [Eq. \(3\)](#)

Step7-6: then

Bray-Curtis (BC) calculate the sum of absolute differences between features relative to their total sum

using [Eq. \(4\)](#)

Step7-7: **END**

Step8: **Return the computed distance values for HamD, JaD, BB, and BC.**

Step9: **END**

RIKP-RS recognition performance. A description of them can be found in [Table 2](#) Five binary similarities are explained.

The proposed RIKP-RS is detailed and outlined in [Algorithm 1](#), which provides a comprehensive step-by-step breakdown of the preprocessing for the IKP detection method, the feature extraction based on two models and the matching and similarity by distance compute. This algorithm serves as the basis for the implementation of the RIKP-RS, demonstrating how to build the database for sub-images of every component and configure the network using two models to achieve the desired results.

4. Experimental results

The presented section covers the evaluation results of the IKP segmentation method as well as the concatenated fusion feature evaluations based on two Model Deep Learning Neural Networks (DLNN) for IKP as well as the overall performance evaluation of the RIKP-RS. The experiments were conducted on a computer with 11th Gen Intel Core i7-13620H processor, 16 GB of RAM, a 512GB SSD NVME for hard disk drive (HDD) and Windows 11 which is a good amount for running Python 3.9 and handles data-intensive operations. Python libraries like PyTorch

Table 2. Show list of similarity metric.

Association measure name, ref	Symbol	Definition	Components of the Equation
Hamming Distance [54, 55]	HamD	$HamD(x, y) = \sum_{i=1}^n 1_{x_i \neq y_i}$	(1) Where, x & y : The two strings or binary sequences, n : the length of strings (or sequences), x_i & y_i : the elements (bits) at the i -th position in the strings x and y
Jaccard Distance [55, 56]	JaD	$J(A, B) = \frac{ A \cap B }{ A \cup B }$	(2) Where: A and B two sets, $ A \cap B $ is the number of common elements in both sets. $ A \cup B $ is the total number of unique elements in both sets.
Braun-Blanquet Distance [53, 56]	BB	$S(A, B) = \frac{ A \cap B }{\max(A , B)}$	(3) Where: $ A \cap B $ is the number of common elements in both sets. $ A $ $ B $ are the sizes (cardinalities) of sets A and B . $\max(A , B)$ is the size of the larger set.
Bray-Curtis Distance [57, 58]	BC	$S_{BC} = \frac{(b + c)}{2a + b + c}$	(4) Where, a , b , and c : represent the abundance of features

Table 3. A demonstrative the accuracy for 11K hands dataset.

11k hand dataset	Actual	Predicate	Accuracy
IKP left Hand-11k Hand dataset	2624	2624	100%
IKP Right Hand-11k Hand dataset	2845	2845	100%

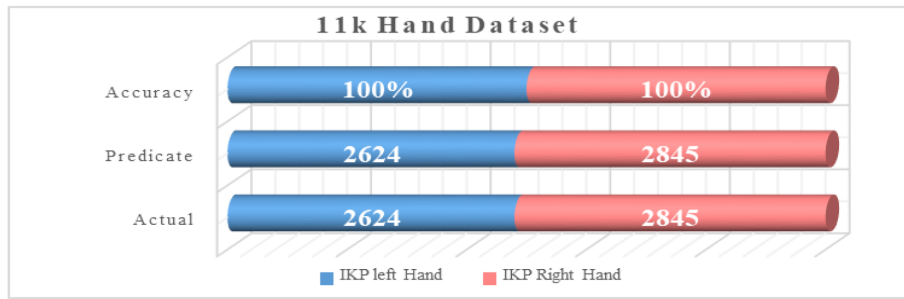


Fig. 4. Show result accuracy for 11K hands dataset.

and TensorFlow benefit from Nvidia GPUs’ performance for deep learning and machine learning.

4.1. Evaluation of the segmentation method

This subsection evaluates the results of the IKP segmentation methods that were suggested during the pre-processing phase. The accuracy for both the right and left hands using the hands’ landmark model is displayed in Table 3.

Our results show that the left-IKP in the 11k Hands dataset produced better and more excellent results than the right-IKP in the 11k Hands dataset. The highest accuracy was described by the actual and predicate for all samples in the 11K Hands dataset in Fig. 4.

4.2. Evaluation of model deep learning neural network (DLNN)

Using two basic models in our experiment IKP features were extracted using “Convolution Neural

Network” (CNN) pretrained. The results of the multimodal deep learning neural network (DLNN) will be evaluated in this subsection: By adding each model’s fine-tuning to the extracted features, the DenseNet201 and Inception V3 models will be evaluated. Evaluating the performance of the IKP involved using multiple metrics: recall, accuracy (ACC), precision (PPV), recall (sensitivity), Specificity(SPC), and F1_score, which were computed using the following Eqs. (5) to (9) [59–63].

$$Accuracy(ACC) = \frac{Tp + Tn}{Tp + Tn + Fp + Fn} \tag{5}$$

$$Precision(PPV) = \frac{Tp}{Tp + Fp} \tag{6}$$

$$Recall(Sensitivity) = \frac{Tp}{Tp + Fn} \tag{7}$$

$$Specificity(SPC) = \frac{Tn}{Tn + Fp} \tag{8}$$

$$F1_Score = \frac{2 * Tp}{2 * Tp + Fp + Fn} \tag{9}$$

Table 4. Analysis accuracy and F1-score fine-tuning denseNet201 model (IKP Right).

	Summarized-Classification-Train			Summarized-classification-Testing		
	Micro%	Macro%	Weighted%	Micro%	Macro%	Weighted%
Precision	86.23	89.83	90.14	85.71	84.38	89.24
Recall	86.23	85.71	86.23	85.71	81.25	85.71
F1-Score	86.23	85.00	85.63	85.71	81.15	87.86
Accuracy	86.23	86.23	86.23	85.71	85.71	85.71

Table 5. Analysis accuracy and F1-score fine tuning DenseNet201 model (IKP Left).

	Summarized-Classification-Train			Summarized-classification-Testing		
	Micro%	Macro%	Weighted%	Micro%	Macro%	Weighted%
Precision	92.86	88.71	96.43	89.88	86.13	88.39
Recall	92.86	88.17	92.86	89.88	86.43	89.88
F1-Score	92.86	87.63	93.25	89.88	85.02	88.52
Accuracy	92.86	92.86	92.86	89.88	89.88	89.88

Table 6. Analysis accuracy and F1-score fine-tuning Inception V3 model (IKP right).

	Summarized-Classification-Train			Summarized-classification-Testing		
	Micro%	Macro%	Weighted%	Micro%	Macro%	Weighted%
Precision	97.21	97.26	97.34	94.05	95.37	95.31
Recall	97.21	97.13	97.21	94.05	93.61	94.05
F1-Score	97.21	97.09	97.18	94.05	93.59	93.84
Accuracy	97.21	97.21	97.21	94.05	94.05	94.05

Table 7. Analysis accuracy and F1 score-fine-tuning Inception V3 model (IKP Left).

	Summarized-Classification-Train			Summarized-classification-Testing		
	Micro%	Macro%	Weighted%	Micro%	Macro%	Weighted%
Precision	99.92	99.54	99.54	99.54	99.51	99.51
Recall	99.92	99.23	99.21	99.54	99.21	99.21
F1-Score	99.92	99.17	99.19	99.54	99.08	99.19
Accuracy	99.92	99.21	99.21	99.54	99.17	99.15

Where: TP refers to True Positive, TN refers to True Negative, FP refers to False Positive, FN refers to False Negative.

4.3. DenseNet201 model's evaluation

The primary dataset is split into training, validation, and testing classes. The suggested models are trained using training data and validated against the validation set at the end of each training cycle. The models are then evaluated using the testing dataset, and the performance of the DenseNet201 is measured utilizing evaluation metrics. Tables 4 and 5 illustrate the results of classification metrics for summarized classification for the DenseNet201 Model (IKP Right) and (IKP Left).

4.4. Inception V3 model's evaluation

Utilizing the testing dataset, the models are evaluated, and the performance of the Inception V3 model is evaluated using evaluation measures. Tables 6

and 7 illustrate the results of classification metrics for summarized classification for the Inception V3 Model (IKP Right) and (IKP Left).

In these tables observed result higher and excellent in Summarized-Classification for every key component in both 11k right and left inner hands dataset in denseNet201 model and Inception V3 model. Fig. 5 presents accuracy and F1-score for every IKP using the DenseNet201 model and Inception V3 Model.

The DenseNet201 and InceptionsV3 models were trained to classify right palmar and left palmar hands are 2845 and 2624 images. Initially, images of size 224×224 pixels were utilized as the input to the models and trained for 100 epochs. The accuracies, F1_score, loss, recall, and precision obtained on the training, validation sets are presented in Figs. 6 and 7 The efficiency of each model's evaluation using the Confusion matrix is shown in Fig. 8.

4.5. Similarity and matching evaluation

Evaluating the similarity between two sub-images of the same hand is one step in the matching process.

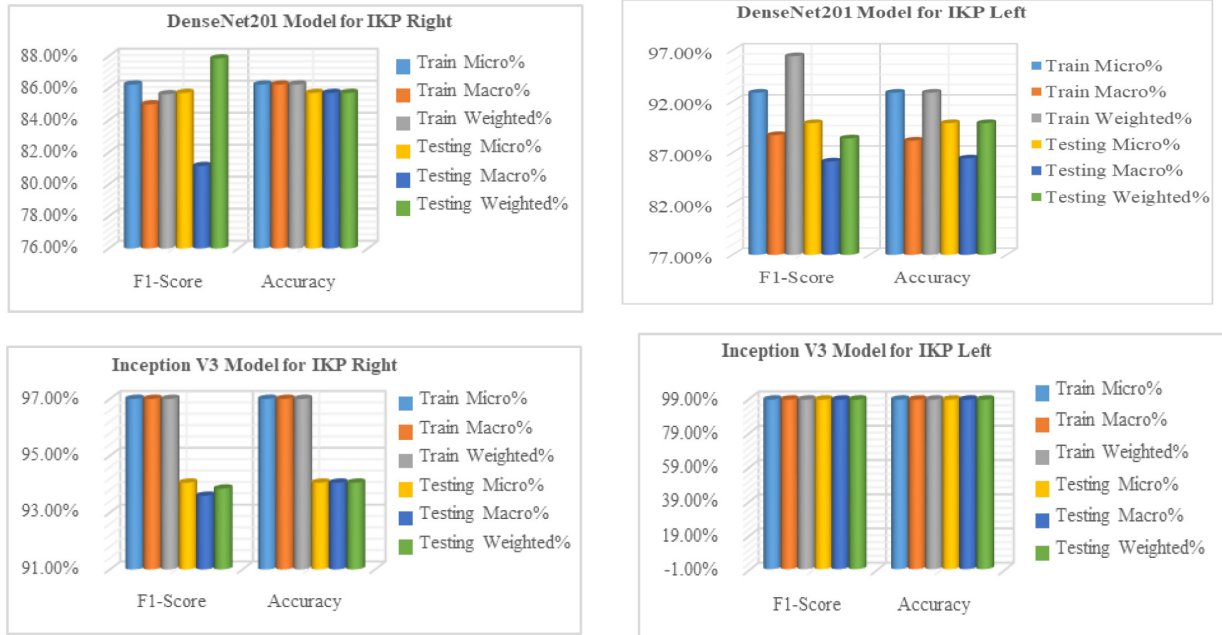


Fig. 5. Comparative line chart for training & testing in DenseNet201 and InceptionV3 models (IKP right & IKP left 11k hands) in proposed system.

During the matching process, one segmented image from the query can match one or more corresponding segmented images in the library. A rank-1 recognition rate was used to evaluate the similarity using the feature vectors acquired in the preceding phase. The rank-1 of recognition is defined as follows:

$$\text{rank} - 1 = \frac{N_i}{N} \times 100 \quad (10)$$

There were a total of N samples that were considered for recognition, and N_i samples were correctly assigned to the right individual. Table 8 displays the rank-1 recognition rate of an 11k hands database as a percentage utilizing multiple pre-trained models and similarity distances.

5. Discussion results

In order to evaluate the effectiveness and robustness of the proposed RIKP-RS, the detection on the actual and predicate images is first compared, as displayed in Table 3, to discuss the accuracy of IKP detection on the 11K Hands dataset. Concerning IKP detection for both hands, our right IKP and left IKP performed best for the highest accuracy. The recognition accuracy is evaluated for the IKP detection method, through many steps affect the feature extraction and recognition accuracy. Hand image blurring is the initial step in the preprocessing phase, can be important, considering that light blurring can help

decrease noise and improve patterns, but exaggerated blurring may disguise curves of the finger, lines of the palm, and details of movement, resulting in reducing recognition accuracy. our proposed RIKP-RS takes considered balancing the level of hand image blurring to maintain substantial features as well as reduce irrelevant details to obtain optimal feature extraction and robust recognition accuracy. Then, utilizing HSV color space to separate skin regions in hand images affects the improvement of feature extraction and recognition accuracy by improving skin detection under different illumination conditions. On the contrary to RGB color space, where HSV uses the hue component to differentiate skin tones, saturation, and value channels to minimize shadows and brightness variations. This results in more accurate to extract the region skin, and improved biometric recognition accuracy. Next, morphological operations (Dilation and Erosion) greatly affect the improvement of extraction features and recognition accuracy, by improving significant structures by filling gaps and connecting fractured hand outlines to strengthen essential components for the dilation process. As well as eliminating noise, and some undesirable details, and enhancing segmentation for the Erosion process. After that, utilizing median filtering will decrease impulse noise while maintaining significant edges and details and this filter improves the clarity of hand contours, making it easier to extract important features for inner knuckle prints for robust recognition accuracy. Finally, in the preprocessing phase

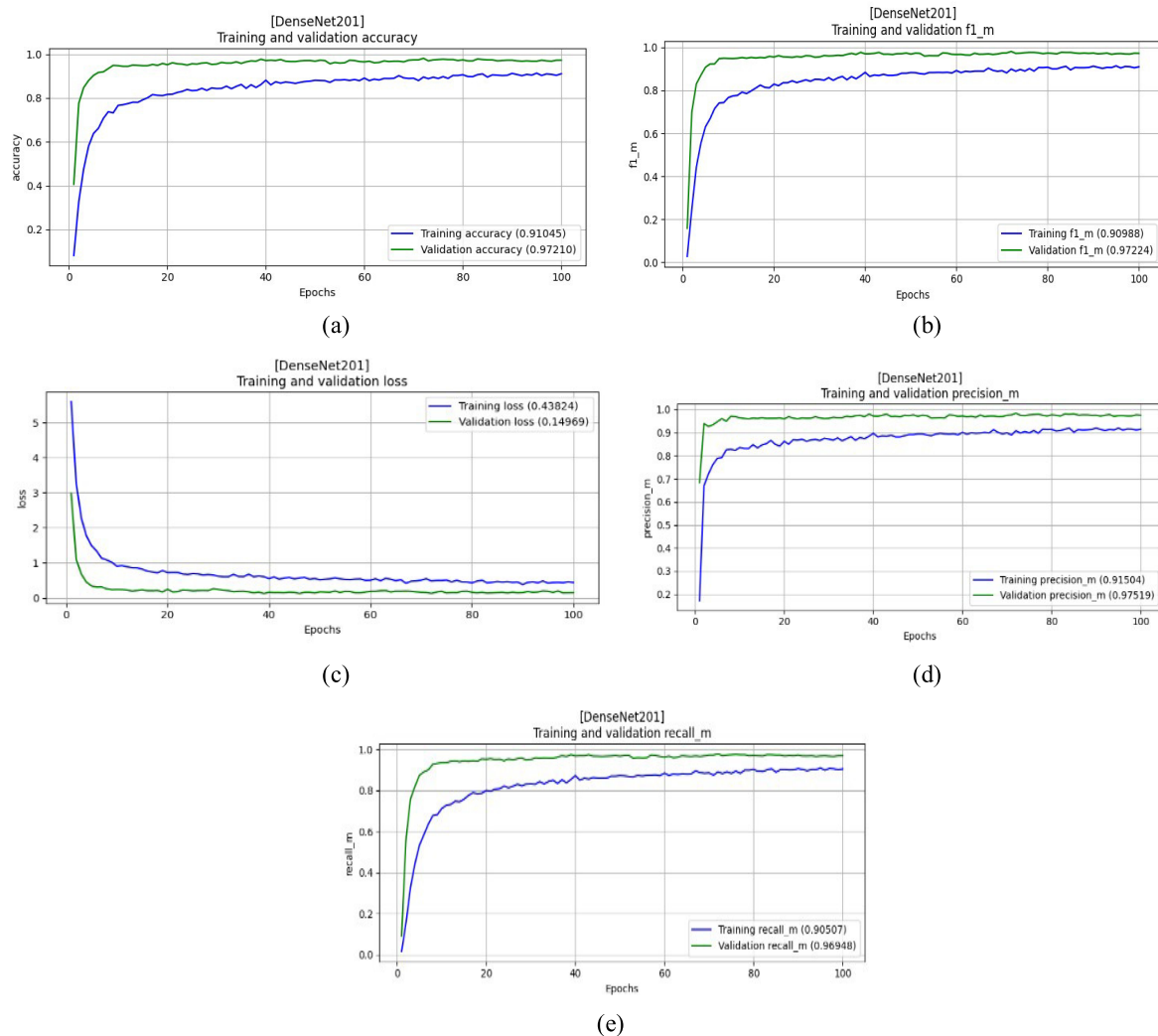


Fig. 6. Show result for DensNet201 model (Some sample for IKP left): (a) Training accuracy & validation accuracy (b) Training F1-Score & validation F1-Score (c) Training loss & validation loss (d) Training precision & validation precision (e) Training recall & validation recall.

use MediaPipe Module that works to improve extract features and recognition accuracy for inner knuckle prints by providing a robust real-time hand tracking and landmark detection framework. It precisely identifies key components of the inner surface of the hand like inner knuckle prints for little finger, ring finger, middle finger, index finger, and thumb finger. To handle hand orientation, illumination, and background noise, MediaPipe Module built-in pose estimation and multi-hand tracking improve recognition accuracy. The performance might operate differently depending on illumination and occlusions.

According to our experiments, multimodal deep learning is the most effective model for recognizing individuals among inception V3 and denseNet201 models, independent of fine-tuning models. The Inception V3 model was found to outperform the DenseNet201 model in extracting abstract and

high-level features on both the 11k right and left inner hands dataset in tables (4, 5, 6, and 7) in section (Inception V3 Model's Evaluation). The F1_score for the denseNet201 model on IKP Right is 87.86%, while the F1_score for the inception V3 model on IKP Left is 88.52%. In contrast, the F1_score is 93.84% for the Inception V3 model on IKP Right, and 99.19% for the inception V3 model on IKP Left. This is because the denseNet201 model has many advantages, requires fewer parameters and processing time, and scales to hundreds of layers automatically without causing any optimization issues. The most accurate and effective model for processing input images when compared to Inception V3 is this one. It is always being improved and is now more effective at recognizing specific images, patterns, and features.

During the matching process, the proposed RIKP-RS uses four distances, where each distance affects on

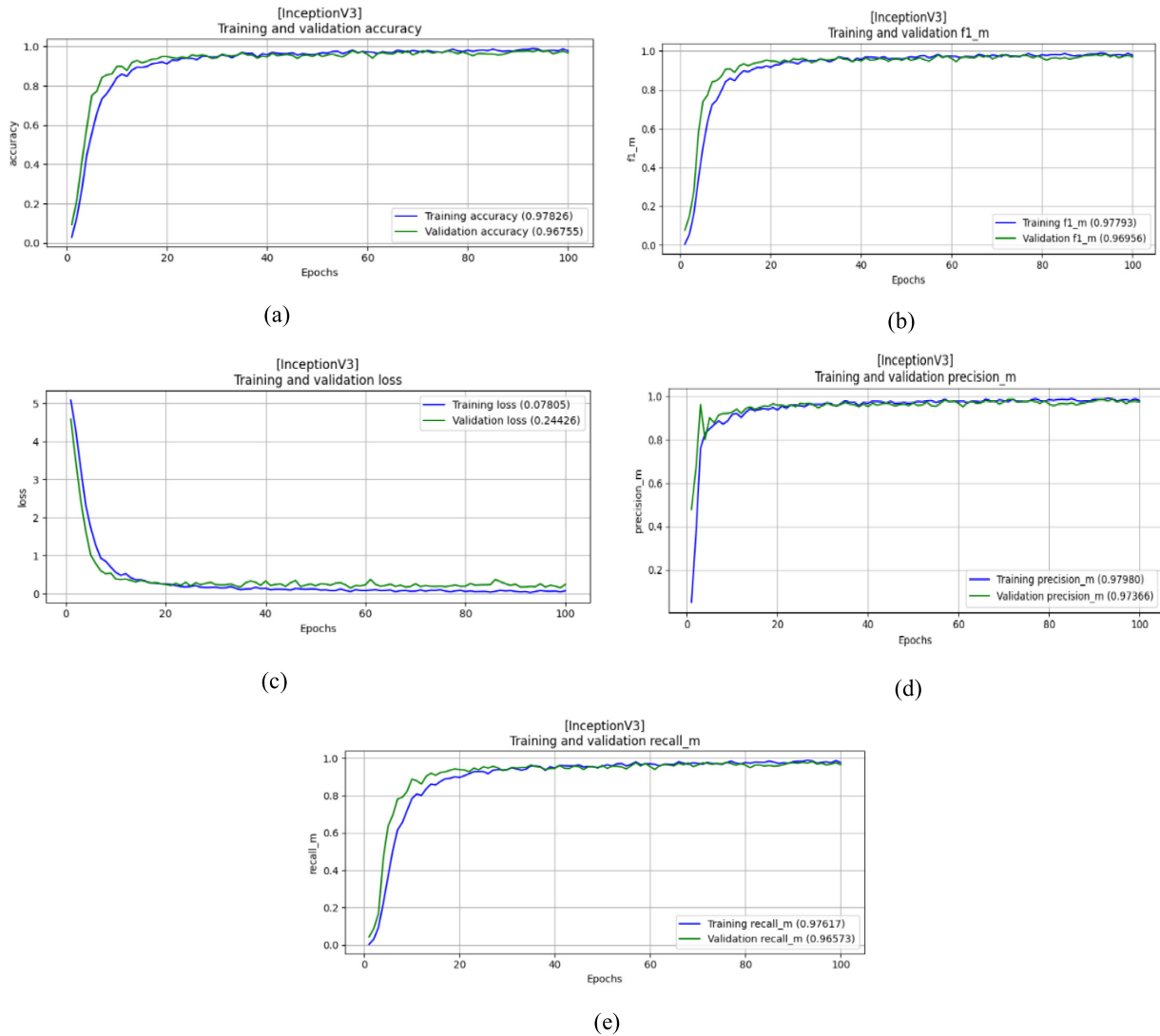


Fig. 7. Show result for Inception V3 model (Some sample for IKP right): (a) Training accuracy & validation accuracy (b) Training F1-Score & validation F1-Score (c) Training loss & validation loss (d) Training precision & validation precision (e) training recall & validation recall.

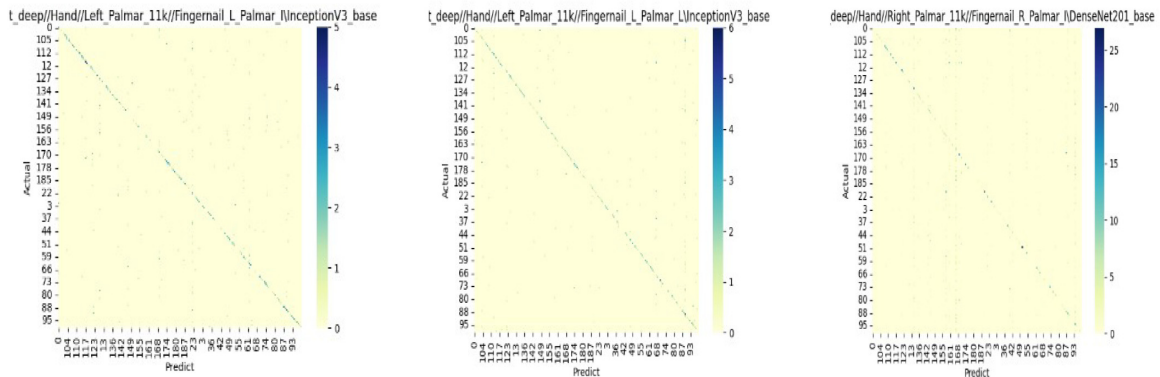


Fig. 8. Confusion matrix for the proposed system for some samples 11K Hands DenseNet201 model & InceptionV3 model.

Table 8. Show the rank-1 recognition rate for the 11k hands (IKP right & IKP left) dataset.

11K Hand Dataset				
Multimodal	DenseNet201-(IKP Right)	InceptionV3-(IKP Right)	DenseNet201-(IKP Left)	InceptionV3-(IKP Left)
Distance	Basic-Little (Rank-1)		Basic-Little (Rank-1)	
HamD	68.59	71.61	69.41	70.48
JaD	85.88	85.53	87.64	90.57
Braun-Blanquet	79.01	82.39	83.50	87.55
Bray-Curtis	85.62	86.20	87.41	90.75
HamD	Basic-Ring (Rank-1)		Basic-Ring (Rank-1)	
JaD	69.59	72.36	70.41	73.41
Braun-Blanquet	83.67	90.02	85.68	93.15
Bray-Curtis	79.63	87.58	80.32	90.75
HamD	Basic-Middle (Rank-1)		Basic-Middle (Rank-1)	
JaD	83.40	84.39	84.73	86.27
Braun-Blanquet	70.37	72.24	71.52	72.07
Bray-Curtis	73.56	74.45	75.56	85.42
HamD	Basic-Index (Rank-1)		Basic-Index (Rank-1)	
JaD	79.03	82.23	81.63	84.98
Braun-Blanquet	84.66	86.28	88.03	90.11
Bray-Curtis	69.56	70.01	70.87	70.17
HamD	78.53	80.22	81.82	84.04
JaD	82.20	87.53	86.07	90.07
Braun-Blanquet	80.83	85.65	86.05	88.73
Bray-Curtis	Basic-Thumb (Rank-1)		Basic-Thumb (Rank-1)	
HamD	67.37	69.62	70.60	72.05
JaD	83.99	85.49	85.76	86.75
Braun-Blanquet	85.49	86.76	86.77	88.85
Bray-Curtis	82.36	83.15	87.73	87.57
HamD	Major-Little (Rank-1)		Major-Little (Rank-1)	
JaD	70.91	71.27	71.46	74.89
Braun-Blanquet	80.63	84.20	86.91	88.60
Bray-Curtis	94.20	96.10	85.43	87.51
HamD	Major-Ring (Rank-1)		Major-Ring (Rank-1)	
JaD	98	99.14	100	100
Braun-Blanquet	84.91	85.62	89.48	91.39
Bray-Curtis	89.86	92.96	87.40	89.52
HamD	Major-Middle (Rank-1)		Major-Middle (Rank-1)	
JaD	95.35	96.76	99.14	99.26
Braun-Blanquet	100	100	100	100
Bray-Curtis	74.52	78.19	85.94	87.57
HamD	Major-Index (Rank-1)		Major-Index (Rank-1)	
JaD	85.58	88.69	88.87	91.97
Braun-Blanquet	87.75	88.28	80.95	90.19
Bray-Curtis	97.13	98	100	100
HamD	Major-Thumb (Rank-1)		Major-Thumb (Rank-1)	
JaD	88.78	99.88	81.58	90.61
Braun-Blanquet	83.67	85.52	92.01	92.49
Bray-Curtis	75.83	79.85	97.58	80.43
HamD	Minor-Little (Rank-1)		Minor-Little (Rank-1)	
JaD	98.38	99.05	99.29	100
Braun-Blanquet	71.10	71.34	70.20	71.39
Bray-Curtis	81.34	84.21	90.42	91.95
HamD	Minor-Index (Rank-1)		Minor-Index (Rank-1)	
JaD	77.84	81.14	83.54	88.23
Braun-Blanquet	88.27	90.29	95.76	97.34
Bray-Curtis	71.87	71.94	70.32	72.52
HamD	Minor-Thumb (Rank-1)		Minor-Thumb (Rank-1)	
JaD	79.40	83.48	88.46	89.27
Braun-Blanquet	74.57	77.25	79.75	86.24
Bray-Curtis	87.02	89.97	88.76	90.13

(Continued)

Table 8. Continued

11K Hand Dataset				
Multimodal	DenseNet201-(IKP Right)	InceptionV3-(IKP Right)	DenseNet201-(IKP Left)	InceptionV3-(IKP Left)
	Minor-Ring (Rank-1)		Minor-Ring (Rank-1)	
HamD	78.81	71.06	81.70	81.17
JaD	77.58	81.70	83.05	87.92
Braun-Blanquet	77.13	77.28	79.07	85.57
Bray-Curtis	83.18	85.69	84.67	85.58
	Minor-Middle (Rank-1)		Minor-Middle (Rank-1)	
HamD	69.48	72.31	71.22	75.47
JaD	78.92	82.27	85.78	87.93
Braun-Blanquet	74.58	77.24	79.03	80.45
Bray-Curtis	79.16	81.11	95.48	99.86
	Minor-Index (Rank-1)		Minor-Index (Rank-1)	
HamD	70.53	73.18	72.36	74.19
JaD	78.55	81.65	89.78	90.59
Braun-Blanquet	80.97	84.99	84.20	85.95
Bray-Curtis	100	100	100	100
	All-Left-IKP		All-Right-IKP	
HamD	71.34	79.15	80.62	82.96
JaD	84.88	87.52	89.07	88.69
Braun-Blanquet	88.37	90.51	90.10	94.75
Bray-Curtis	96.68	98.32	98.45	99.81

matching process. The first similarity distance HamD is used to achieve simple, efficient and enhanced accuracy by quickly identifying subtle mismatches in the feature vector (FV), although its performance may degrade when dealing with continuous data where subtle variations are necessary. The second similarity distance JaD focuses only absence-presence of features, efficiency, reduces noise, and irrelevant differences, resulting in a more robust and precise discernment among classes. This distance can be a great improvement in recognition accuracy, especially when distinguishing between real matches from partial overlaps is essential. The third similarity distance BB is best suited for enhanced recognition accuracy in pattern recognition such as inner knuckle prints (IKP) through distinguishing patterns that may appear identical when utilizing binary measures. Finally, the similarity distance BC is used because it efficiently measures the relative among feature distributions, and is robust to an imbalanced dataset which is useful for an IKP recognition system. The rank-1 recognition accuracy in both IKP hands is acquired by computing the results of similarity distances (Hamming distance (HamD), Jaccard distance (JaD), Braun-Blanquet (BB), and Bray-Curtis (BC)). The highest results were observed in almost concatenated fusion for the IKP left hand compared to the IKP right hand, and the Inception V3 model outperformed the DenseNet201 model in matching measurements. It was also noticed through experiments with both IKP-Basic, IKP-Major, and IKP-Minor that the IKP-Major achieved the best

results while ranking second for IKP-minor and third for IKP-minor, where the rank_1 (100%) for DenseNet 201 model and Inception V3 model in IKP-Major left for fingers (Little Finger, Ring Finger, and Middle Finger), the rank_1 (100%) for DenseNet 201 model and Inception V3 model in IKP-Major right for Ring finger, and the rank_1 (100%) for DenseNet 201 model and Inception V3 model in IKP-Minor right for Index finger as well as rank_1 achieved used Bray-Curtis (BC) distance on concatenated fusion for IKP, the rank_1 (98.45%) for DenseNet201 Model in IKP-All Left, the rank_1 (99.81%) for InceptionV3 Model in IKP-All Left, the rank_1 (96.68%) for DenseNet201 Model in IKP-All Left, the rank_1 (98.32%) for InceptionV3 Model in IKP-All Left for each finger (Little Finger, Ring Finger, Middle Finger, Index Finger, and Thumb Finger) and as has been listed in Table 8. By comparing IKP for Basic, Major, and Minor for DenseNet201 Model and InceptionV3 Model using four distances, the BC distance achieved the best results while ranking second for BB distance, ranking third for Ham distance and fourth JaD distance as indicated in Fig. 9.

The pioneering system of the proposed RIKP-RS is highlighted in Table 9 by comparing it with various previous studies. Compared to other systems, our system's results demonstrated a higher recognition accuracy than those of other previous studies. This system clearly outperforms existing methods when compared to key elements including datasets, Classifier, FE models, and preprocessing.



Fig. 9. The rank₁ for the proposed (RIKP-RS) and compare between the rank₁ recognition for the DenseNet201 Model & InceptionV3 Model for right and left hands in the 11k Hands.

Table 9. Comparison of the proposed RIKP-RS with selected previous studies.

Ref.	Preprocessing	Feature Extraction	Classifier	Number of fingers and Modalities	Results
[16]	ROI extraction, employs a detection strategy that ranges from coarse to fine.	ALLBP	Hamming Distance (HamD)	3 Finger (Basic + Minor)	FRR = 0%, FAR = 0.03%
[17]	Grayscale image, Noisy image, and Normalized image (Use Median filter)	LLBP	ANN + SVM	1 Finger (Middle Finger)	Accuracy = 89%, and 97%
[20]	ROI extraction smooths the noisy image, normalizes the brightness of the image	MMCP	Normalized Hamming Distance (HamD)	3 Finger (Major)	EER = 0.36%
[21]	ROI extraction, Gray IKPs, Estimated coarse reflections, Uniform Brightness IKPs, Enhanced IKPs		NDI, and Chi-Square	4 Finger (Center Knuckle (Major))	EER = 0.92 ± 0.35 BIR = 98.91 ± 0.63
[24]	ROI extraction, and CLAHE	LDP, Diagonal PCA, and IKP Geometrical Features	K-NN classifier	2 Finger (Major)	CRR = 96%, and EER = 3.45%
[25]	ROI extraction, Harris corner detection, and K-means clustering algorithm	Geometric Features for (12 centroids and 4 fingertips)	K-NN for Compute Euclidean Distance (ED)	-	RR = 98.39%
[26]	Crop the wrist and other terminals, Convert to a binary image, Rotate and extract the 4 finger images	CV + DWT	NN	4 Finger (Finger Inner Side (FIS) Pattern)	FAR = 0.3333%, and FRR = 0.8889%
[28]	Binarization, Morphological Processing, Contour Extraction, Corner Positioning, Finger Separation, and ROI extraction		CNN	-	RR = 95.2%
[29]	Guided Filter (Smoothed version), hand extracted and normalized	CNN	SVM	-	Avg. Acc = 0.942 and 0.973)
Our Proposed RIKP-RS	Blurring Hand Images, Convert to HSV Color Space, Morphological Operations (Dilation and Erosion), Median Filtering, and MediaPipe Module	Concatenated Fusion IKP Features using Fine-Tuning DenseNet201 Model + Fine-Tuning Inception V3 Model	Hamming Distance(HamD), Jaccard Distance (JaD), Braun-Blanquet (BBD), and Bray Curtis Distance (BCD)	5 Finger (Basic, Minor, Major)	F1-Score = 98.45%, 99.81%, 96.68%, and 98.32%

6. Conclusion

In this given work, a robust system for inner knuckle print recognition named RIKP-RS is proposed and implemented on the 11K Hands dataset. The proposed system uses the palmer surface of the fourteen inner knuckle hand components (Basic (5), Major (4), Minor (4)). The system provides segmentation methods based on the advanced MediaPipe Module. The

system motivates feature-level inner knuckle print for all fingers based on fine-tuning multi-model deep learning, with inner knuckle print (IKP) playing an important role in individual recognition. The proposed RIKP-RS was evaluated on datasets of hand images captured with closed, half-closed, and widely open. Utilizing the proposed system always increases recognition accuracy, as the biometric procedure uses the concatenated fusion of all inner knuckle print

(IKP) or inner knuckle print (IKP) separately. The RIKP-RS suffers from limitations in some of the key components (basic and Minor) of the fingers (Ring, Middle, and thumbs) in the matching distance of the features vector, where although it achieves good results, it is weak compared to the other fingers since the parameter value selection inappropriate value for DenseNet201 and Inception V3 Models, in addition, some samples of the basic hand component in this 11K hand dataset need for perform more preprocessing steps on the hand images, these limitations are a subject of future research, in addition to researching more intricate feature extraction models, such as the resnet50 and mobile Net V3 Large models, and using of 11K Hand dorsal datasets; attempts are already being made to develop these proposed datasets. The main objective of these measures is to increase the system's robustness even more.

Authors' declaration

- Conflicts of Interest: None.
- We hereby confirm that all the Figures and Tables in the manuscript are ours. Furthermore, any Figures and images, that are not ours, have been included with the necessary permission for republication, which is attached to the manuscript.

Authors' contribution statement

H.S.C., and T.A. participated in proposing the research idea, the significant roles that each researcher played can be summed up as follows: The author H.S.C. find relevant sources, collected the dataset and configured the final folders of each category, and designed the multimodal, including the architecture of the deep learning for each models, make descriptive tables, and analyze the results and tables. On the other hand, researcher T.A. played a major role in drawing the figures, writing algorithms, the grammatical aspect, the linguistic aspect, minimizing plagiarism and quoting, determining the scientific methodology of the research, determining the initial research directions, and directly supervise the intellectual and scientific material of the article.

References

1. M. Oudah, A. Al-Naji, and J. Chahl, "Hand gesture recognition based on computer vision: A review of techniques," *Journal of Imaging*, vol. 6, no. 8, p. 73, 2020. <https://doi.org/10.3390/jimaging6080073>.
2. W. Wu, S. J. Elliott, S. Lin, S. Sun, and Y. Tang, "Review of palm vein recognition," *IET Biometrics*, vol. 9, no. 1, pp. 1–10, 2020. <https://doi.org/10.1049/iet-bmt.2019.0034>.
3. R. V. Adiraju, K. K. Masanipalli, T. D. Reddy, R. Pedapalli, S. Chundru, and A. K. Panigrahy, "An extensive survey on finger and palm vein recognition system," *Materials Today: Proceedings*, vol. 45, pp. 1804–1808, 2021. <https://doi.org/10.1016/j.matpr.2020.08.742>.
4. G. Jaswal, A. Kaul, and R. Nath, "Knuckle print biometrics and fusion schemes—overview, challenges, and solutions," *ACM Computing Surveys (CSUR)*, vol. 49, no. 2, pp. 1–46, 2016. <https://doi.org/10.1145/2938727>.
5. A. S. Tarawneh *et al.* "Deepknuckle: Deep learning for finger knuckle print recognition," *Electronics*, vol. 11, no. 4, p. 513, 2022. <https://doi.org/10.3390/electronics11040513>.
6. K. H. Cheng and A. Kumar, "Deep feature collaboration for challenging 3D finger knuckle identification," *IEEE Transactions on Information Forensics and Security*, vol. 16, pp. 1158–1173, 2020. <https://doi.org/10.1109/tifs.2020.3029906>.
7. A. Attia, S. Mazaa, Z. Akhtar, and Y. Chahir. 2022, "Deep learning-driven palmprint and finger knuckle pattern-based multimodal person recognition system," *Multimedia Tools and Applications*, vol. 81, no. 8, pp. 10961–10980, 2022. <https://doi.org/10.1007/s11042-022-12384-3>.
8. J. Khodadoust, M. A. Medina-Pérez, R. Monroy, A. M. Khodadoust, and S. S. Mirkamali, "A multibiometric system based on the fusion of fingerprint, finger-vein, and finger-knuckle-print," *Expert Systems with Applications*, vol. 176, p. 114687, 2021. <https://doi.org/10.1016/j.eswa.2021.114687>.
9. L.-Q. Zhu and S.-Y. Zhang, "Multimodal biometric identification system based on finger geometry, knuckle print and palm print," *Pattern Recognition Letters*, vol. 31, no. 12, pp. 1641–1649, 2010. <https://doi.org/10.1016/j.patrec.2010.05.010>.
10. L. Jiang, X. Liu, H. Wang, and D. Zhao, "Finger vein and inner knuckle print recognition based on multilevel feature fusion network," *Applied Sciences*, vol. 12, no. 21, p. 11182, 2022. <https://doi.org/10.3390/app122111182>.
11. S. Ribaric and I. Fratric, "A biometric identification system based on eigenpalm and eigenfinger features," *IEEE Transactions on Pattern Analysis and Machine Intelligence*, vol. 27, no. 11, pp. 1698–1709, 2005. <https://doi.org/10.1109/tpami.2005.209>.
12. M. K. Goh, C. Tee, and A. B. Teoh, "Bi-modal palm print and knuckle print recognition system," *Journal of IT in Asia*, vol. 3, no. 1, pp. 85–106, 2010. <https://doi.org/10.33736/jita.37.2010>.
13. B. Bhaskar and S. Veluchamy, "Hand based multibiometric authentication using local feature extraction," In *2014 International Conference on Recent Trends in Information Technology*, 2014, IEEE, pp. 1–5. <https://doi.org/10.1109/icrtit.2014.6996136>.
14. H. Yi, D. Xiusheng, S. Shiyu, and C. Zhigang, "A study on deep neural networks framework," In *2016 IEEE Advanced Information Management, Communicates, Electronic and Automation Control Conference (IMCEC)*, IEEE, 2016, pp. 1519–1522. <https://doi.org/10.1109/IMCEC.2016.7867471>.
15. M. Liu, Y. Tian, and Y. Ma, "Inner-knuckle-print recognition based on improved LBP," In *Proceedings of the 2012 International Conference on Information Technology and Software Engineering: Software Engineering & Digital Media Technology*, Springer, 2013, pp. 623–630. <https://doi.org/10.1049/bme2.12000>.
16. F. Bahmed and M. Ould Mammam, "Basic finger inner-knuckle print: A new hand biometric modality," *IET Biometrics*, vol. 10, no. 1, pp. 65–73, 2021. <https://doi.org/10.1049/bme2.12000>.

17. H. R. N and C. P. K, "Inner knuckle print identification using artificial neural network," *International Journal of Advanced Information and Communication Technology*, vol. 7, no. 8, pp. 115–118, 2020. <https://doi.org/10.46532/ijaict-2020025>
18. M. Viswanathan, G. B. Loganathan, and S. Srinivasan, "IKP based biometric authentication using artificial neural network," In *AIP Conference Proceedings*, AIP Publishing, 2020, vol. 2271, no. 1. <https://doi.org/10.1063/5.0025229>.
19. W. Li, "[Retracted] biometric recognition of finger knuckle print based on the fusion of global features and local features," *Journal of Healthcare Engineering*, vol. 2022, no. 1, p. 6041828, 2022. <https://doi.org/10.1155/2022/6041828>.
20. Z. Tao, Y. Hu, and X. Wang, "A new biometric system based on inner-knuckle-print recognition," In *IOP Conference Series: Earth and Environmental Science*, IOP Publishing, 2019, vol. 252, no. 3, p. 032210. <https://doi.org/10.1088/1755-1315/252/3/032210>.
21. M. A. Sadik, M. N. Al-Berry, and M. Roushdy, "A robust alignment-based personal recognition using center inner Knuckle prints," In *2017 Eighth International Conference on Intelligent Computing and Information Systems (ICICIS)*, IEEE, 2017, pp. 84–91. <https://doi.org/10.1109/intelcis.2017.8260037>.
22. F. K. Nezhadian and S. Rashidi, "Inner-knuckle-print for human authentication by using ring and middle fingers," In *2016 2nd International Conference of Signal Processing and Intelligent Systems (ICSPIS)*, IEEE, 2016, pp. 1–6. <https://doi.org/10.1109/icspis.2016.7869849>.
23. A. Kazemtarghi, F. Kharajinezhadian, and S. Rashidi, "Personal authentication using inner knuckle print based on RGB images," In *2017 24th National and 2nd International Iranian Conference on Biomedical Engineering (ICBME)*, IEEE, 2017, pp. 1–6. <https://doi.org/10.1109/icbme.2017.8430234>.
24. G. Jaswal, A. Kaul, and R. Nath, "IKP based human authentication using multi-feature fusion," In *2017 4th International Conference on Signal Processing and Integrated Networks (SPIN)*, IEEE, 2017, pp. 154–159. <https://doi.org/10.1109/spin.2017.8049935>.
25. Y. Zhu, Yu. Wang, Y. Zheng, and M. Wu, "Identification method of inner knuckle print based on geometric features," In *2023 6th International Conference on Communication Engineering and Technology (ICCET)*, IEEE, 2023, pp. 154–160. <https://doi.org/10.1109/ICCET58756.2023.00034>.
26. R. R. O. Al-Nima, N. A. Al-Obaidy, and L. A. Al-Hbati, "Segmenting finger inner surface for the purpose of human recognition," In *2019 2nd International Conference on Engineering Technology and its Applications (IICETA)*, IEEE, 2019, pp. 105–110. <https://doi.org/10.1109/iiceta47481.2019.9012985>.
27. R. Al-Nima, S. S. Dlay, W. L. Woo, and J. A. Chambers, "Human authentication with finger textures based on image feature enhancement," 2015. <https://doi.org/10.1049/cp.2015.1784>.
28. Y. Xue, M. Liu, M. Qiao, and M. Xue, "Research on inner knuckle pattern recognition method based on convolutional neural network," In *2021 IEEE 5th Advanced Information Technology, Electronic and Automation Control Conference (IAEAC)*, IEEE, vol. 5, 2021, pp. 2510–2513. <https://doi.org/10.1109/IAEAC50856.2021.9390697>.
29. M. Afif, "11K hands: Gender recognition and biometric identification using a large dataset of hand images," *Multimedia Tools and Applications*, vol. 78, pp. 20835–20854, 2019. <https://doi.org/10.1007/s11042-019-7424-8>.
30. A. Kumar and Z. Xu, "Personal identification using minor knuckle patterns from palm dorsal surface," *IEEE Transactions on Information Forensics and Security*, vol. 11, no. 10, pp. 2338–2348, 2016. <https://doi.org/10.1109/tifs.2016.2574309>.
31. M. Diarra, A. K. Jean, B. Bakary, and K. B. Médard, "Study of deep learning methods for fingerprint recognition," *International Journal of Recent Technology and Engineering (IJRTE)*, vol. 10, no. 3, pp. 192–197, 2021. <https://doi.org/10.35940/ijrte.C6478.0910321>.
32. F. Zhuang et al. "A comprehensive survey on transfer learning," *Proceedings of the IEEE*, vol. 109, no. 1, pp. 43–76, 2020. <https://doi.org/10.1109/JPROC.2020.3004555>.
33. C. E. Floyd Jr, J. Y. Lo, A. J. Yun, D. C. Sullivan, and P. J. Kornguth, "Prediction of breast cancer malignancy using an artificial neural network," *Cancer: Interdisciplinary International Journal of the American Cancer Society*, vol. 74, no. 11, pp. 2944–2948, 1994. [https://doi.org/10.1002/1097-0142\(19941201\)74:11 < 2944::AID-CNCR2820741109 > 3.0.CO;2-F](https://doi.org/10.1002/1097-0142(19941201)74:11 < 2944::AID-CNCR2820741109 > 3.0.CO;2-F).
34. M. Liu, M. Yi, M. Wu, J. Wang, and Y. He, "Breast pathological image classification based on VGG16 feature concatenation," *Journal of Shanghai Jiaotong University (Science)*, vol. 27, no. 4, pp. 473–484, 2022. <https://doi.org/10.1007/s12204-021-2398-x>.
35. A. Rafiq et al. "Detection and classification of histopathological breast images using a fusion of CNN frameworks," *Diagnostics*, vol. 13, no. 10, p. 1700, 2023. <https://doi.org/10.3390/diagnostics13101700>.
36. G. Huang, Z. Liu, L. Van Der Maaten, and K. Q. Weinberger, "Densely connected convolutional networks," In *Proceedings of the IEEE Conference on Computer Vision and Pattern Recognition*, pp. 4700–4708, 2017.
37. C. Szegedy, V. Vanhoucke, S. Ioffe, J. Shlens, and Z. Wojna, "Rethinking the inception architecture for computer vision," In *Proceedings of the IEEE Conference on Computer Vision and Pattern Recognition*, pp. 2818–2826, 2016. <https://doi.org/10.1109/cvpr.2016.308>.
38. R. Yan and L. Shao, "Blind image blur estimation via deep learning," *IEEE Transactions on Image Processing*, vol. 25, no. 4, pp. 1910–1921, 2016. <https://doi.org/10.1109/TIP.2016.2535273>.
39. H. Yamaura, M. Tamura, and S. Nakamura, "Image blurring method for enhancing digital content viewing experience," In *Human-Computer Interaction. Theories, Methods, and Human Issues: 20th International Conference, HCI International 2018, Las Vegas, NV, USA, July 15–20, 2018, Proceedings, Part I 20*, Springer, 2018, pp. 355–370. https://doi.org/10.1007/978-3-319-91238-7_29.
40. V. Chernov, J. Alander, and V. Bochko, "Integer-based accurate conversion between RGB and HSV color spaces," *Computers & Electrical Engineering*, vol. 46, pp. 328–337, 2015. <https://doi.org/10.1016/j.compeleceng.2015.08.005>.
41. D. Giuliani, "Metaheuristic algorithms applied to color image segmentation on HSV space," *Journal of Imaging*, vol. 8, no. 1, pp. 6, 2022. <https://doi.org/10.3390/jimaging8010006>.
42. F. S. Hassan and A. Gutub, "Improving data hiding within colour images using hue component of HSV colour space," *CAA Transactions on Intelligence Technology*, vol. 7, no. 1, pp. 56–68, 2022. <https://doi.org/10.1049/cit2.12053>.
43. K. A. M. Said and A. B. Jambek, "Analysis of image processing using morphological erosion and dilation," In *Journal of Physics: Conference Series*, IOP Publishing, 2021, vol. 2071, no. 1, p. 012033. <https://doi.org/10.1088/1742-6596/2071/1/012033>.
44. S. Raju and E. Rajan, "Skin texture analysis using morphological dilation and erosion," *Int. J. Pure Appl. Math*, vol. 118, pp. 205–223, 2018.
45. J. E. Rodríguez and D. Ayala, "Erosion and dilation on 2-D and 3-D digital images: A new size-independent approach," In *VMV*, 2001.

46. B. Justusson, "Median filtering: Statistical properties," *Two-dimensional Digital Signal Processing II: Transforms and Median Filters*, pp. 161–196, 2006. <https://doi.org/10.1007/bfb0057597>.
47. H. Soni and D. Sankhe, "Image restoration using adaptive median filtering," *Image*, vol. 6, no. 10, 2019.
48. K. O. Boateng, B. W. Asubam, and D. S. Laar, "Improving the effectiveness of the median filter," 2012.
49. R. Kumar, A. Bajpai, and A. Sinha, "Mediapipe and cnns for real-time asl gesture recognition," *arXiv preprint arXiv:2305.05296*, 2023.
50. G. Amprimo, G. Masi, G. Pettiti, G. Olmo, L. Priano, and C. Ferraris, "Hand tracking for clinical applications: Validation of the google mediapipe hand (GMH) and the depth-enhanced GMH-D frameworks," *Biomedical Signal Processing and Control*, vol. 96, p. 106508, 2024. <https://doi.org/10.1016/j.bspc.2024.106508>.
51. K. Usha and M. Ezhilarasan, "Personal recognition using finger knuckle shape oriented features and texture analysis," *Journal of King Saud University-Computer and Information Sciences*, vol. 28, no. 4, pp. 416–431, 2016. <http://doi.org/10.1016/j.jksuci.2015.02.004>.
52. K. Usha and M. Ezhilarasan, "Fusion of geometric and texture features for finger knuckle surface recognition," *Alexandria Engineering Journal*, vol. 55, no. 1, pp. 683–697, 2016. <https://doi.org/10.1016/j.aej.2015.10.003>.
53. S. S. Choi, S. H. Cha, and C. C. Tappert, "A survey of binary similarity and distance measures," *Journal of Systemics, Cybernetics and Informatics*, vol. 8, no. 1, pp. 43–48, 2010.
54. Y. Bo, A. Soni, S. Srivastava, and M. Khosla, "Evaluating representational similarity measures from the lens of functional correspondence," *arXiv preprint arXiv: 2411.14633*, 2024.
55. R. Todeschini, V. Consonni, H. Xiang, J. Holliday, M. Buscema, and P. Willett, "Similarity coefficients for binary chemoinformatics data: Overview and extended comparison using simulated and real data sets," *Journal of Chemical Information and Modeling*, vol. 52, no. 11, pp. 2884–2901, 2012. <https://doi.org/10.1021/ci300261r>.
56. M. Paradowski, "On the order equivalence relation of binary association measures," *International Journal of Applied Mathematics and Computer Science*, vol. 25, no. 3, pp. 645–657, 2015. <https://doi.org/10.1515/amcs-2015-0047>.
57. Y. Sari, M. Alkaff, and R. A. Pramunendar, "Iris recognition based on distance similarity and PCA," In *AIP Conference Proceedings*, AIP Publishing, vol. 1977, no. 1, 2018. <https://doi.org/10.1063/1.5042900>.
58. R. Shyam and Y. N. Singh, "Recognizing individuals from unconstrained facial images," In *Intelligent Systems Technologies and Applications*, Springer, vol. 1, pp. 383–392, 2016. https://doi.org/10.1007/978-3-319-23036-8_33
59. K. Shaker and A. Alqudsi, "Approach for detecting arabic fake news using deep learning," *Iraqi Journal for Computer Science and Mathematics*, vol. 5, No. 3, pp. 779–789, 2024. <https://doi.org/10.52866/ijcsm.2024.05.03.049>
60. D. Hemanand, P. Mohankumar, N. M. Kumar, S. Vaitheki, and P. Saranya, "An intelligent prairie dog optimization (IPDO) and deep auto-neural network (DANN) based IDS for WSN security," *Iraqi Journal for Computer Science and Mathematics*, vol. 4, no. 4, pp. 30–42, 2023. <https://doi.org/10.52866/ijcsm.2023.04.04.004>.
61. O. M. Abdulaziz and O. A. Saltykova, "CNN-PS: Electroencephalogram classification of brain states using hybrid machine - deep learning approach," *Iraqi Journal for Computer Science and Mathematics*, vol. 4, no. 4, pp. 63–75, 2023. <https://doi.org/10.52866/ijcsm.2023.04.04.006>.
62. L. N. Faraj, B. M. Albaker, and Asmaa H. Rasheed, "Machine learning versus deep learning for contact detection in human-robot collaboration," *Al-Iraqia Journal for Scientific Engineering Research*, vol. 3, no. 3, 2024. <http://doi.org/10.58564/IJSER.3.3.2024.234>.
63. S. M. Hameed and Z. H. Ali, "SMS spam detection based on fuzzy rules and binary particle swarm optimization," *International Journal of Intelligent Engineering & Systems*, vol. 14, no. 2, 2021. <http://doi.org/10.22266/ijies2021.0430.28>.